CHEMISTRY
A EUROPEAN JOURNAL

DOI: 10.1002/chem.200701861

Frequency-Dependent Alternating-Current Scanning Electrochemical Microscopy (4D AC-SECM) for Local Visualisation of Corrosion Sites

Kathrin Eckhard,[a] Thomas Erichsen,[a] Martin Stratmann,[b] and Wolfgang Schuhmann*[a]

Abstract: For a better understanding of the initiation of localised corrosion, there is a need for analytical tools that are capable of imaging corrosion pits and precursor sites with high spatial resolution and sensitivity. The lateral electrochemical contrast in alternating-current scanning electrochemical microscopy (AC-SECM) has been found to be highly dependent on the frequency of the applied alternating voltage. In order to be able to obtain data with optimum contrast and high resolution, the AC frequency is swept in a full spectrum at each point in space instead of performing spatially resolved measurements at one fixed perturbation frequency. In doing so, four-dimensional data sets are acquired (4D AC-SECM). Here, we describe the instrument set-up and modus operandi, along with the first results from the imaging of corroding surfaces. Corrosion precursor sites and local defects in protective organic coatings, as well as an actively corroding pit on 304 stainless steel, have been successfully visualised. Since the lateral electrochemical contrast in these images varies with the perturbation frequency, the proposed approach constitutes an indispensable tool for obtaining optimum electrochemical contrast.

Keywords: analytical methods · corrosion · impedance · scanning probe microscopy · surface analysis

Introduction

Since its introduction in 1989, scanning electrochemical microscopy (SECM)[1] has matured to become a ubiquitous tool in local surface analysis.[2,3] In recent years, localised corrosion phenomena have been the subject of increasing attention.[4–7] A number of SECM detection schemes involve the measurement of Faraday currents, as, for example, in amperometric feedback mode,[8] generator–collector mode,[9] or redox competition mode,[10] among others. Some modes, however, do not depend on the occurrence of redox reactions and hence are possible to perform without the addition of a freely diffusing redox mediator. Therefore, they may be used to probe samples without unavoidably influencing them at the same time through the Nernst potential at the sample/electrolyte interface. Examples include local potentiometry[11] and alternating-current scanning electrochemical microscopy (AC-SECM). The latter provides analytical signals that are dependent on the tip-to-sample separation, which is a prerequisite for local microscopy. This feature can be used for precise vertical positioning of SECM tips for amperometric,[12] enzymatic,[13] or potentiometric[14] sensors. The AC signal has been further utilised to establish a constant distance control in SECM,[15] although it should be noted that this is only applicable on electrochemically homogeneous sample surfaces.[16] Furthermore, the alternating current response may be successfully used to monitor variations in the local electrochemical activity of a sample.[17–21] While electrically insulating samples invariably lead to a negative feedback response during z approaches, electrically conducting samples may cause either negative feedback,[15,22] positive feedback,[13,17,20] or both, depending on the experimental conditions.[23,24]

AC-SECM has also been coupled to current-independent distance-control devices, as in piezo–piezo shear force positioning[22,25] and AFM.[24,26] Since the signal is influenced by the local admittance of the solution, it has also been utilised to image ion flux through membrane pores.[27,28] The concept of AC-SECM resembles that of local electrochemical impe-

[a] Dr. K. Eckhard, Dr. T. Erichsen, Prof. Dr. W. Schuhmann
Analytische Chemie—Elektroanalytik und Sensorik
Ruhr-Universität Bochum
Universitätsstrasse 150, 44780 Bochum (Germany)
Fax: (+49) 234-32-14683
E-mail: wolfgang.schuhmann@rub.de

[b] Prof. Dr. M. Stratmann
Max-Planck-Institut für Eisenforschung
Max-Planck-Strasse 1, 40237 Düsseldorf (Germany)

Supporting information for this article is available on the WWW under http://www.chemeurj.org/ or from the author.

dance mapping (LEIM),[29,30] as both approaches implement a type of local microscopy based on the detection of alternating current signals at one single frequency. LEIM is performed in a five-electrode arrangement with a platinised twin-tip akin to that used in local electrochemical impedance spectroscopy (LEIS). In LEIS, full impedance spectra are recorded exclusively at the sites of interest; lateral scanning is only conducted at one frequency. In contrast to LEIS or LEIM, in AC-SECM conventionally designed ultramicroelectrodes (UME) are employed, enabling straightforward adoption of the technique and good prospects for improved resolution by miniaturisation of the probe.[25] Thus, based on our previous developments with respect to the generation of four-dimensional data sets in SECM,[10,31] we now demonstrate the implementation of frequency scans at each *x*,*y* position of the scanning electrochemical microscope. In this paper, an instrument is introduced that combines the detailed information of frequency spectroscopy with the spatial resolution of local microscopy.

Results and Discussion

The dependences of the positive feedback[23,24] and of the lateral electrochemical contrast[24] on the perturbation frequency in AC-SECM have been described previously. The threshold frequency for positive feedback behaviour to occur over conductive samples varies with specific experimental conditions, such as the nature of the sample, the ionic strength of the electrolyte, and the active diameter of the SECM tip. This has obvious consequences for the quality of lateral imaging in AC-SECM. An arbitrarily chosen frequency might conceal features in the local distribution of electroactivity. Similarly, recording full-frequency spectra before scanning at only a few spots could miss the point of interest on unknown sample surfaces. It follows that the way to proceed is to combine the advantages of spatially resolved activity mapping with automated sweeps in the perturbation frequency in order to obtain the optimum electrochemical contrast.

Therefore, based on an existing AC-SECM instrument, the concept that is outlined schematically in Scheme 1 has been realised.[17] At each point in space, the applied frequency is changed through the digital communication between the PC and lock-in amplifier (LIA) according to user-defined parameters. It can be swept from low to high values or vice versa in either linear or logarithmic increments.

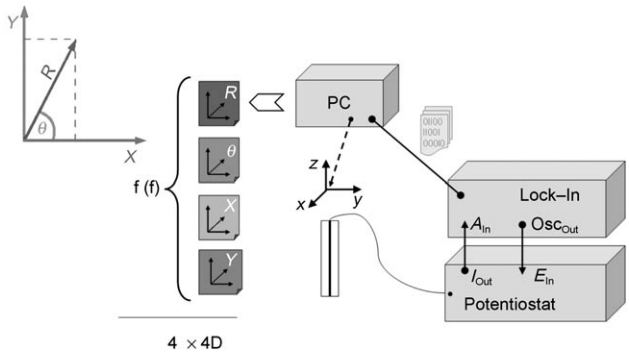

Scheme 1. Schematic outline of the experiment. The ultramicroelectrode is scanned in the *x* and *y* directions across a sample. Communication with the computer (PC) is achieved through a serial port of the digital lock-in amplifier (LIA). The lateral distribution of the current magnitude R (as well as the phase shift and real and imaginary parts of the alternating current response) is acquired as a function of frequency, resulting in four-dimensional data sets.

The required sampling times for each current value are inversely proportional to the perturbation frequency. The time needed to record a full spectrum depends on the frequencies and the number of increments, and for a spectrum of 50 frequencies between 100 Hz and 100000 Hz takes about 8 s at each point in space. The resulting alternating current response is acquired digitally as a function of the applied frequency. Thereby, spectra proportional to the complex admittance are obtained and stored together with the coordinates of the tip position.

An experimental example of such a spectrum is shown in Figure 1A (squares). It was recorded with a 10 μm diameter UME in bulk solution ($c = 1$ mM $NaClO_4$) in the frequency range from 273 Hz to 96.485 kHz with a perturbation amplitude of 0.1 V. At first, the current magnitude rises with increasing frequency, then reaches a maximum, before decaying once more. Considering the simplest equivalent circuit for an electrochemical cell in the absence of any redox mediator, that is, a resistor and a capacitor in series, the experi-

Abstract in German: *Um die Entstehung lokaler Korrosionsphänomene untersuchen zu können, bedarf es ortsauflösender Methoden, die beispielsweise Lochfraß oder Korrosionsvorstufen mit hoher lateraler Auflösung visualisieren können. Bei der Abbildung lokaler elektrochemischer Aktivität mittels wechselstrombasierter elektrochemischer Rastermikroskopie (AC-SECM) ist der Kontrast in hohem Maße abhängig von der gewählten Anregungsfrequenz. Um den Informationsgehalt der erhaltenen Bilder zu erhöhen und optimalen elektrochemischen Kontrast zu erzielen, wird vorgeschlagen, an jedem Punkt des Rastergitters, ein komplettes Frequenzspektrum aufzunehmen, anstatt die Oberfläche mit einer einzigen, willkürlich gewählten Anregungsfrequenz abzurastern. Dadurch werden vierdimensionale Datensätze erhalten (4D AC-SECM). Wir berichten hier über den Aufbau des neu entwickelte Instrumentes, seine Funktionsweise und über erste Ergebnisse zur Abbildung korrodierender Oberflächen. Korrosionsvorstufen und Defekte in organischen Schutzschichten konnten ebenso erfolgreich visualisiert werden wie ein Korrosionsherd auf einer 304 Edelstahl-Oberfläche. Die hier vorgestellte Herangehensweise garantiert die Erfassung des optimalen elektrochemischen Kontrastes und damit eine hohe Auflösung bei der Visualisierung korrodierender Oberflächen.*

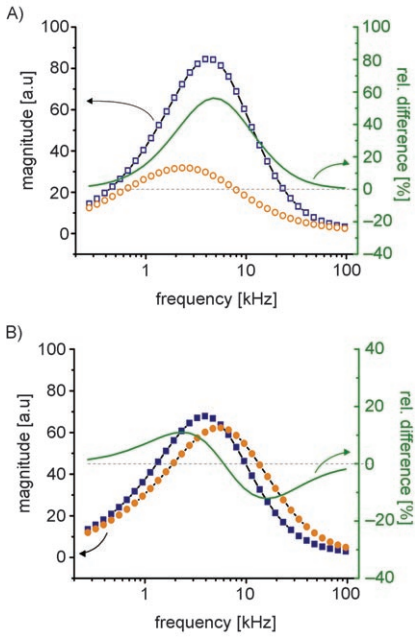

Figure 1. Frequency spectra from 96485 to 273 Hz recorded over samples of SiO_2 (A) and Au (B) with the SECM tip positioned close to the sample surface (○/●) and in bulk solution (□/■); $c = 1$ mM $NaClO_4$, $d = 10$ μm, $V_{pp} = 100$ mV.

mental data are at variance with what one might expect. At low frequencies, the double layer represented by the capacitor dominates the overall cell impedance and hence the current response signal is small. Since the impedance of the capacitance is inversely proportional to the frequency, the current initially increases with rising perturbation frequency. Beyond a characteristic threshold frequency, the capacitor should no longer contribute to the overall cell impedance.[23,24] In that case, the overall cell impedance would be expected to remain constant, given that the resistor is independent of the frequency. The observed decay in current magnitude for higher frequencies up to 100 kHz is caused by inevitable stray capacitances. For this reason, Ervin et al.[27] decided to work at frequencies lower than 1.5 kHz to exclude influences by wires and electrical connections. In high-frequency regions, the effective bandwidth of the current follower or potentiostat can also become the limiting factor. Diakowski et al.[23] therefore calibrated their instrumentation for each current range of the current follower with known resistors for each frequency. The resulting mathematical corrections were small for low frequencies, but became significant at high frequencies.

In order to investigate the influences of the vertical tip position and the nature of the underlying sample, frequency spectra were recorded over samples of glass (Figure 1A) and gold (Figure 1B), respectively. For both samples, the SECM tip was positioned once at the near-field distance (circles) and once in bulk solution (squares).

The data recorded over glass display a significant decrease of the current magnitude compared to the bulk solution signal when the electrode tip is positioned near the sample surface. This is due to the blocking nature of the insulating glass sample, which leads to a negative-feedback-type response during z approach. The SECM tip and sample at a small separation from one another form a highly resistive thin-layer cell.[32] The impedance of the tip increases as the electrolyte film trapped between tip and sample becomes thinner. Thus, the inversely proportional alternating current magnitude decreases. Hence, at each frequency, the magnitude of the current at tip positions close to the surface (circles; Figure 1A) is smaller than that in the bulk solution (squares; Figure 1A). At a given frequency, the absolute difference between the bulk spectrum and the spectrum obtained with the tip positioned close to the gold surface is much smaller (Figure 1B). Moreover, the two spectra intersect, so that at higher frequencies the current magnitudes at the surface are in fact larger than those in bulk solution. This corresponds to a positive-feedback-type response over electrically conducting surfaces.

The developed instrument was utilised to obtain z-approach curves while simultaneously changing the perturbation frequency at each spatial position automatically. For instance, during one individual z-approach experiment, 34 z-approach curves at different perturbation frequencies were obtained, a small selection of which are displayed in Figure 2. Figure 2A shows the current magnitude during z approach towards an SiO_2 surface, while Figure 2B shows the corresponding data on approaching an Au surface. As can be deduced from Figure 2, insulating samples result in purely negative feedback approach curves for all perturbation frequencies, while conducting samples also allow positive feedback responses. The conducting substrate offers an alternative pathway for the alternating current, so that the highly resistive thin-layer electrolyte can be partially circumvented. At high perturbation frequencies, the overall cell impedance even decreases, resulting in an increase in the current magnitude close to the sample surface. This flip from negative feedback to positive feedback approach curves over conducting sites has been described previously.[23,24]

In the case of insulating sample surfaces (Figure 2A), the perturbation frequency has a gradual effect on the shape of the z-approach curve. Compared to the bulk solution results, the current magnitude signal alters most drastically upon approaching at frequencies between about 6 and 13 kHz. Smaller changes in the relative signal are seen at both higher and lower frequencies. However, there is still a qualitative difference to be revealed by this experiment. Comparing the approach curves obtained at 1352 or 2754 Hz with that obtained at 33.199 kHz (Figure 2A), it becomes obvious that very high frequencies show a much larger near-field distance. At high frequencies such as 33.199 kHz, the shape of the approach curve is rather flat, but the interaction with the surface extends several tens of micrometers into the solution. Therefore, high-frequency measurements ought to be less sensitive to changes in surface topography. The approach at 1352 Hz, however, decreases within a mere 15 μm (the electrode diameter was 25 μm). Nonetheless, as already

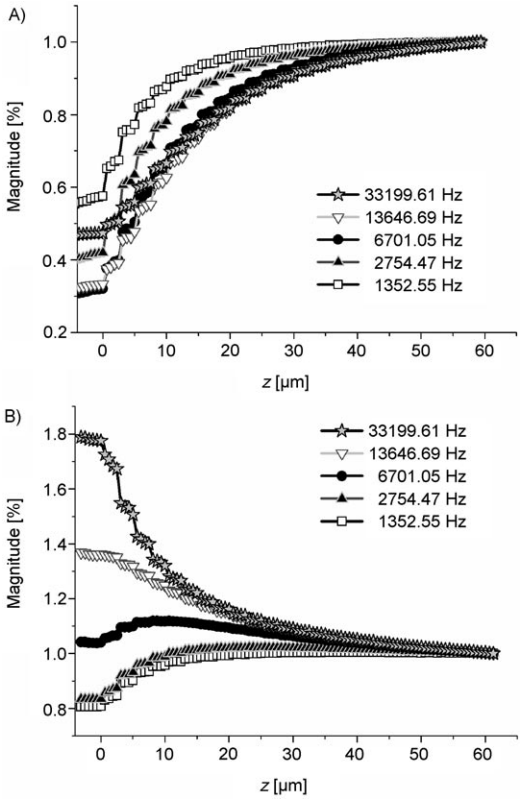

Figure 2. Approach curves towards SiO_2 (A) and Au (B) surfaces. At each point in space, the frequency was swept automatically from 273 Hz to 96485 Hz in 33 increments; $c=1$ mM $NaClO_4$, $d=10$ μm, $V_{pp}=100$ mV. A selection of the resulting current approach curves is plotted for the frequencies indicated.

expected from Figure 1, all z-approach curves towards an insulating surface result in negative feedback behaviour. On the contrary, in the case of a conducting sample, the direction of the feedback response changes with frequency (Figure 2B). Low frequencies cause negative feedback, while high frequencies lead to positive feedback responses.

The detection scheme in AC-SECM depends on measuring the resistance at the tip. However, this resistance can be masked by the impedance of the electrode capacitance in the case of small diameter tips, high ionic strength, or low voltage perturbation frequencies. If the frequency exceeds the time constant of the electrochemical cell, the contribution of the double-layer capacitance to the overall cell impedance of this series RC circuit is suppressed. Hence, high perturbation frequencies lead to a positive feedback response in the z-approach curve (Figure 2B). Thus, the absolute difference between the bulk and surface signals for the Au sample (Figure 1B, solid line) naturally displays two maxima corresponding to negative and positive feedback responses, respectively. It is interesting to note here that the point of zero crossing coincides with the maximum in the absolute difference between the spectra obtained in bulk solution and directly recorded at the insulating glass substrate (Figure 1A, solid line). In Figure 3, curves of the absolute signal drop during z approach are plotted as a function of frequency. Here, the magnitudes of the current and the phase shift with the tip located in close proximity to the sample surface have been subtracted from the corresponding bulk signals. Depending on the applied frequency and the nature of the sample, the magnitude of the signal drop varies greatly. A pronounced signal drop in the near field is desired in scanning probe microscopy to guarantee high-contrast imaging results. However, if the near-field interaction is potentially extinguished under certain parameters, it is difficult to identify a single perturbation frequency suitable for imaging. The maximum signal drop in the current magnitude for approaching an SiO_2 surface under the given conditions occurs at around 8 kHz (Figure 3, solid line).

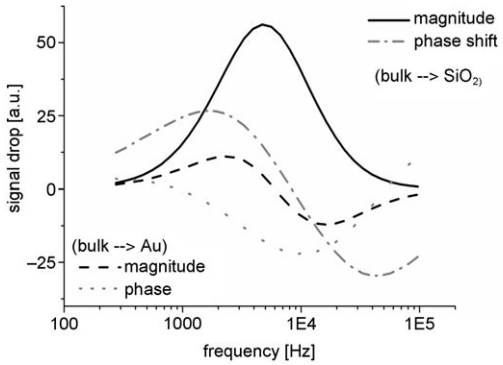

Figure 3. Absolute signal drop during AC-SECM z-approach curves; $c=$ 1 mM $NaClO_4$, $d=10$ μm, $V_{pp}=100$ mV. Displayed are the differences in current magnitude (black) and phase shift (grey) as a function of the perturbation frequency of the applied voltage when approaching glass (solid and dashed lines) and gold (dash-dotted and dotted lines) surfaces. A negative absolute signal drop indicates positive feedback response during the z approach.

Accordingly, the differences in the magnitudes of the signals recorded over an insulator (solid line) and a conductor (dashed line) are large in this frequency range. This kind of distinct difference in signals over insulating and conducting parts of a sample is essential for imaging the local electrochemical surface properties. However, this frequency range of roughly 8 kHz would not have been chosen if the lateral scan had been started over a conducting surface area. At this perturbation frequency, the curves of the current magnitude upon z approach towards an Au surface change under the given conditions from a negative to a positive feedback response. Therefore, the absolute difference in magnitude of the bulk and surface signals is about zero at 8 kHz (Figure 3, dashed line). The frequency at which the feedback response flips from negative to positive changes with the nature and size of the conducting sample, the diameter of the electrode tip, and the ionic strength of the electrolyte (data not shown).

Recording single z approach curves with low vertical contrast over conductors (e.g., $f=8$ kHz on Au) disguises the high lateral electrochemical contrast that could be achieved at this perturbation frequency. Obviously, the frequency for optimum imaging contrast cannot be determined before-

hand for unknown samples. This is especially the case since the phase shift as well as the real and imaginary parts of the alternating current response also display maxima for the signal change during the z approach and the lateral electrochemical contrast at different perturbation frequencies. The phase shifts in the differences between the surface and bulk signals are plotted in Figure 3. The differences obtained over Au (dotted line) and over SiO_2 (dot-dash line) intersect at about 18 kHz. A map of the local phase shift at this perturbation cannot reveal the distribution of electrochemical surface activity. Thus, for optimum lateral contrast, it is vital to perform scans at various perturbation frequencies.[24]

In recognition of this fact, the improved AC-SECM instrument with automatic recording of full-frequency spectra was utilised to scan the surface of a lacquered tin plate as used in the food packaging industry. It was a low-carbon steel galvanised with tin and subsequently covered with a 9–15 μm layer of epoxyphenolic varnish. The insulating polymer layer had deliberately been damaged prior to the experiment in order to expose the underlying metal and, thus, to create sites with increased electrochemical activity. Lateral scans across a sample surface result in 3D maps of the electrochemical surface activity distribution. Since the perturbation frequency is digitally altered at each point of the scanning grid, surface activity images are automatically acquired for multiple frequencies during one single SECM measurement. The resulting four-dimensional data set can be displayed as a movie consisting of several single 3D images as a function of perturbation frequency (please refer to the Supporting Information). Excerpts of these movies are shown in Figure 4.

A circular defect of about 220 μm in diameter, which had been introduced by punching the polymer coating with a needle, was imaged by means of 4D AC-SECM and the result is displayed in Figure 4A. At a perturbation frequency of 273 Hz, the influence of the defect in the coating on the local values of the AC magnitude is seen to extend much further in the x and y directions than the actual size of the defect. This can be attributed to capacitive components, which dominate the signal at this frequency. Defects in protective coatings can lead to dissolution of the underlying tin substrate, thus resulting in a point source from which ions are released into solution, which, in turn, changes the local ionic strength. With increasing perturbation frequency, the visualised defect becomes more confined (Figure 4A). At high frequencies, the predominant contribution to the overall cell impedance is the local impedance of the sample surface. The field lines are able to enter the conducting sample and travel within it with virtually no resistance, finally exiting the sample at a remote place closer to the counter electrode. Therefore, under the given experimental conditions, for perturbation frequencies > 8 kHz, locations with removed and intact organic coating can clearly be distinguished with high spatial resolution. In a second experiment, shown in Figure 4B, larger defects were introduced in the organic layer of a similar sample. Using a scalpel, three parallel scratches were generated perpendicular to the x-scanning direction. At a perturbation frequency of 273 Hz, the signal-to-noise ratio is low and only two scratches are visible (Figure 4B). At 793 Hz, the third defect in the organic layer becomes apparent on the right-hand-side of the image. It is, however, small and displays substantial cross-talk to the scratch in the centre. The images obtained at 2.754 and 8.005 kHz are less noisy and clearly reveal the three defects in the coating. Nonetheless, the current magnitude at tip positions over the intact layer is still influenced by the neighbouring defects. At higher frequencies, this cross-talk of the surface features is further suppressed. At 33.199 kHz, the signal-to-noise ratio is large and the current magnitude between the defects declines to a background value. The surface area that is probed at high perturbation frequencies is much more confined than that at lower frequencies, at which capacitive contributions also contribute to the overall signal. For this reason, the scratches appear to be much broader in the images at $f<1$ kHz. An additional reason for the flat background in the images obtained at high frequencies ($f=8.005$ kHz and 33.199 kHz) is the minimised influence of topographic features. As became apparent from the set of z approach curves in Figure 2A, higher perturbation frequencies result in approach curves with smaller slopes and an increased near-field distance.

For experimental situations like those in Figure 4A,B, that is, a sample surface with mainly insulating areas (organic layer) and local defects (scratches), which are small compared to the size of the sample but large compared to the electrochemically active size of the tip (25 μm), high perturbation frequencies are obviously beneficial. The images become less susceptible to topographic influences, show confined electroactive features at their actual size, and display a high signal-to-noise ratio. These improvements are due to a minimised contribution of the capacitive impedance at higher frequencies. Beyond a certain threshold frequency, the capacitance of the electrode tip is permeable to the alternating current. In this case, the tip resistance is the dominant contribution to the overall impedance of the system, which guarantees optimal electrochemical contrast. This holds true even though the use of high frequencies invariably gives rise to current leaks and stray capacitances (see Figure 1). Despite these features, the lateral electrochemical contrast is significantly improved by choosing high frequencies (Figure 4).

Other experimental designs, however, include a more complex interplay of parameters. On a large (1 cm^2) stainless steel (304 SS) surface, a corrosion pit was initiated using the direct mode of SECM.[33] The sample was mechanically polished in subsequent steps with sandpaper and alumina paste down to a grain size of 1 μm. The configuration is outlined on the left-hand-side of Scheme 2. Here, the SECM tip serves as the counter electrode, while the sample (working electrode) is polarised anodically. Since the counter electrode is smaller than the working electrode by several orders of magnitude, it becomes limiting for the current. Thus, the anodic breakdown of the passive layer on the steel working electrode occurs predominantly in the vicinity of

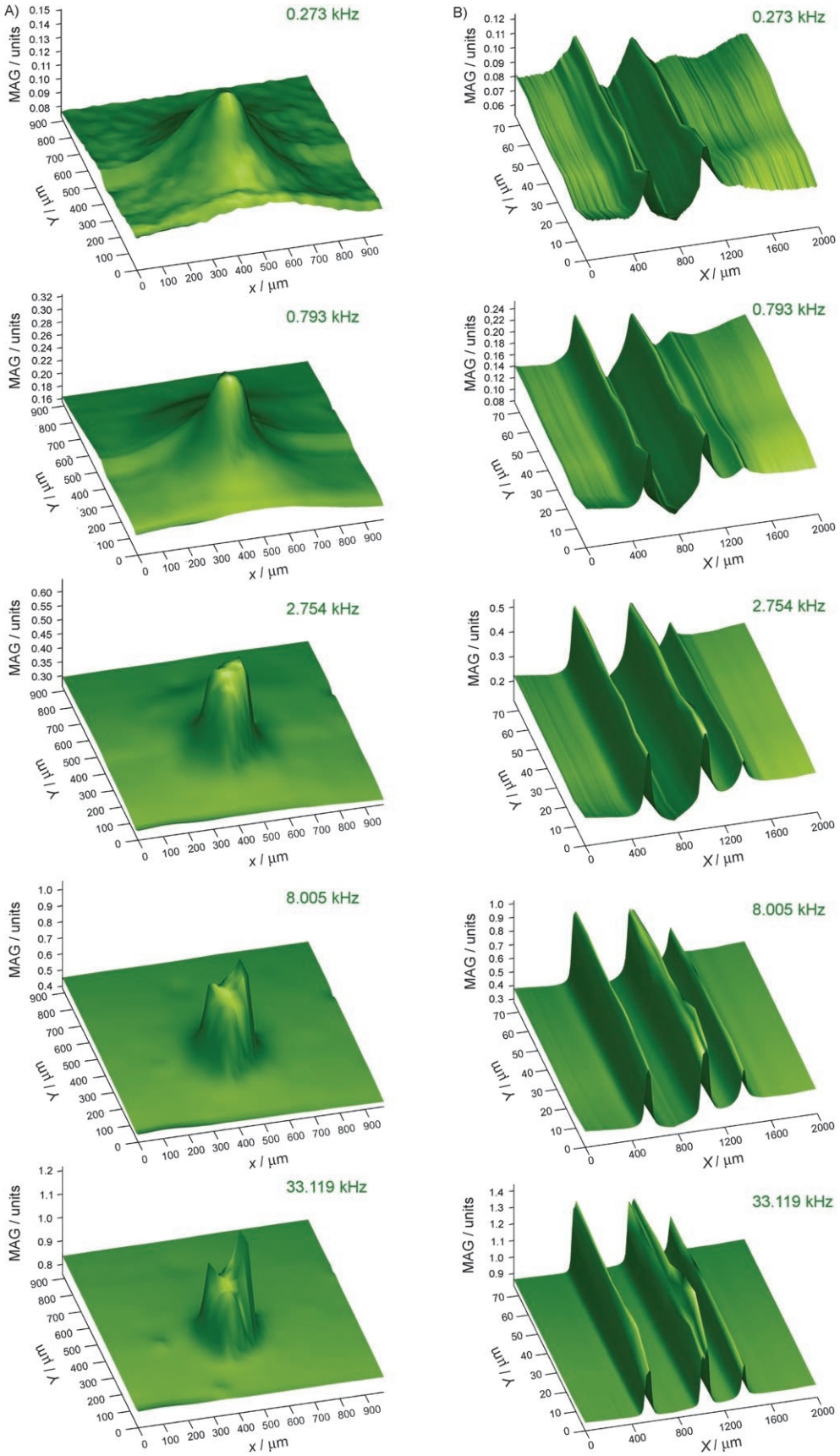

Figure 4. 4D AC-SECM measurements on a lacquered tin plate; $d_{tip}=25$ µm, $c=1$ mM $KClO_4$, $V_{pp}=100$ mV, $f=0.273$ kHz → 33.199 kHz in 27 logarithmic increments. For the animated movie data, refer to the Supporting Information. From top to bottom: 0.273, 0.793, 2.754 kHz, 8.005, 33.199 kHz. A) pinhole, scan area = 1000 µm × 1000 µm; B) scan area = 2000 µm × 80 µm.

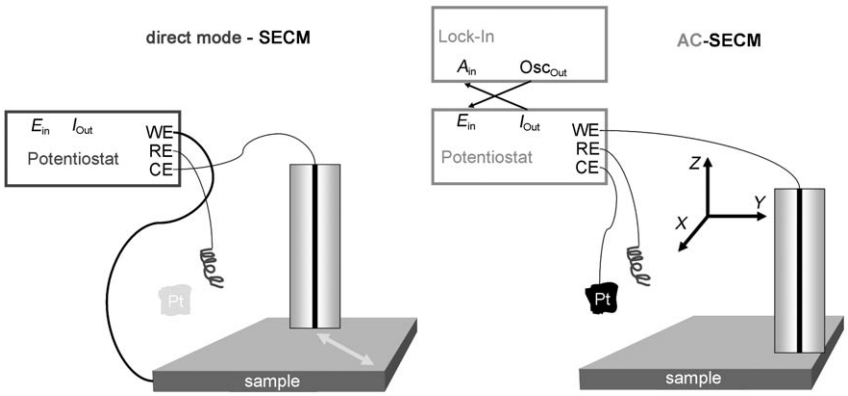

Scheme 2. Schematic outline of the experiment. Use of the electrode arrangement in direct mode (left) was followed by an AC-SECM measurement (right). Direct mode: linear sweep at $\vartheta = 1\ mV s^{-1}$ from 0 mV to 1200 mV vs Ag/AgCl in 1 mM $KClO_4$. AC-SECM: see Figure 5.

Since the sample presents a large metallic surface (1 cm^2) compared to the lacquered tinplate, it also has a large capacitance (C_S and $C_{S'}$). The impedance $Z(C_S)$ is inversely proportional to the capacitance and very low for large sample surfaces. Thus, above a certain threshold frequency, the capacitive pathway through the sample can completely shortcut the working and counter electrodes. Thereby, the local information on the surface resistance ($R_{S'}$) at the position of the SECM tip is lost. Therefore, in this experiment, lower frequencies yield the best lateral electrochemical contrast (Figure 5). When imaging unknown samples, there is no possibility of determining the frequency for optimum contrast in the electrochemical image prior to the lateral scan. The AC perturbation frequency should be high in order to shortcut the capacitance of the tip, but at the same time it must

Knowing the relative position of the actively induced corrosion spot, it can subsequently be visualised by means of 4D AC-SECM.

The same area had been scanned in the AC-SECM mode (Scheme 2, right) before inducing corrosion to ensure that the surface had originally been electrochemically homogeneous (data not shown). The outcome of the subsequent scan is displayed in Figure 5. The spot is located in the centre of the image. At voltage perturbations of 0.501 kHz and 0.987 kHz, the corrosion pit appears as an area of higher current magnitude, represented in white in the false colour image. A frequency of 6.387 kHz caused the current magnitude to decrease over the corrosion spot.

Due to this inversion, the spot is less distinguishable from the background at intermediate frequencies (cf. the images obtained at 1.643 kHz and 2.307 kHz in Figure 5). Interestingly, frequencies that led to the best electrochemical contrast in the experiments presented in Figure 4A,B ($f >$ 20 kHz) do not reveal the corrosion pit at all (cf. the image obtained at 20.949 kHz in Figure 5). This is due to the size of the conducting surface area of the sample. Figure 6 shows a simplified equivalent circuit taking into consideration the properties of the sample. R_{sol} is the solution resistance, which changes with the absolute z distance between the tip and the sample surface. This fact underlies the origin of the near-field response and is, therefore, a prerequisite for successful application of the technique as scanning microscopy. R_T and C_T are the resistance and capacitance of the tip, respectively, while R_S and C_S denote the resistance and capacitance of the sample. $R_{S'}$ and $C_{S'}$ are the resistance and capacitance of the sample at the specific area that is covered by the glass shield of the tip. It can therefore be presumed that the ratio of insulating glass to active electrode size (RG value) of the tip will influence the outcome of the measurement. Similar equivalent circuits have been proposed previously.[19] The local information on the sample is derived from local variations in $R_{S'}$ and its relationship with R_{sol}. The current can either flow through the solution or via the sample.

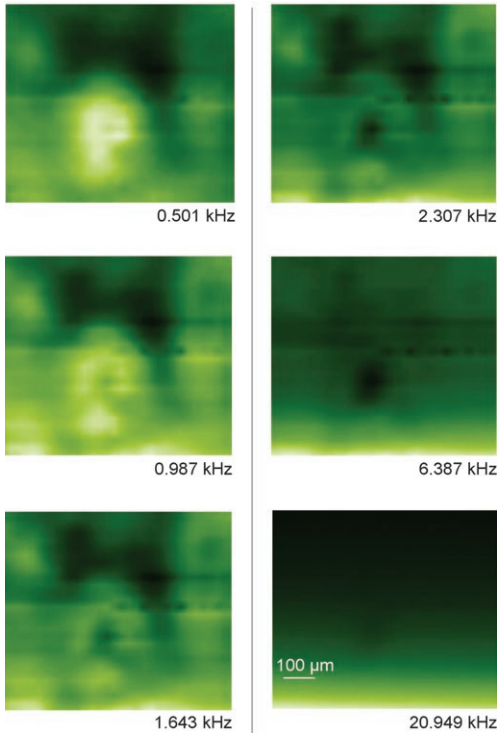

Figure 5. 4D AC-SECM measurements on a 1 cm^2 sample of 304 stainless steel. The surface had been polished down to 1 µm and subsequently anodised in direct mode SECM (see Scheme 2). Scan area = 750 µm × 600 µm, d_{tip} = 25 µm, c = 1 mM $KClO_4$ (fresh), V_{pp} = 100 mV, f = 0.501 kHz → 96.485 kHz in 31 logarithmic increments. 3D maps of this data set are displayed for f = 0.501 kHz, 0.987 kHz, 1.643 kHz (left) and 2.307 kHz, 6.387 kHz, 20.949 kHz (right).

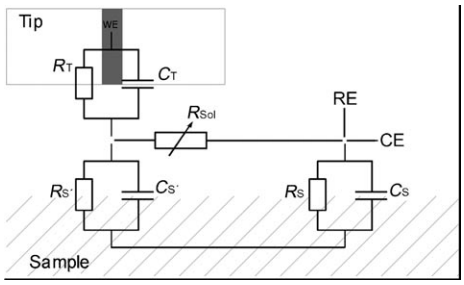

Figure 6. Simplified equivalent circuit of an AC-SECM arrangement scanning a large conductive sample. For further details, refer to the text.

not be so high as to short-cut the capacitance of large conducting sample surfaces. Since the ultimate aim of this work is to investigate unknown structures, the optimum frequency for doing so will always be inherently unknown. The experimental design suggested in this contribution provides an elegant way to circumvent this by collecting data at various frequencies during one single scan.

Conclusion

In view of the frequency dependence of the lateral electrochemical contrast in AC-SECM imaging, a technique is suggested to systematically deal with and take advantage of this phenomenon. The introduced scanning electrochemical microscopy instrument automatically collects frequency spectra at each point in space. This impedance-based procedure gains access to data of high electrochemical content with high spatial resolution. Misinterpretation caused by arbitrarily chosen frequencies for the lateral imaging is methodically avoided. The optimal parameters for imaging are dependent on the geometry and size of the electrode tip, the ionic strength of the solution, and, in the case of conducting sites, also on the size and nature of the sample. The introduced four-dimensional method of frequency-dependent AC-SECM thus represents a straightforward tool for lateral imaging of surface activity at optimal electrochemical contrast. Future work will include the combination of 4D AC-SECM with shear-force based distance control as well as converting the data into complex impedances.

Experimental Section

General: Potassium perchlorate was purchased from Riedel-de-Haen (Seelze, Germany) and was used as received. Solutions were prepared with deionised triply-distilled water. Electrodes were fabricated according to a protocol described previously.[34]

Instrumentation: The instrument was adapted based on the scanning electrochemical microscope employed in ref. [17]. Briefly, it consisted of a step-motor-driven *x*,*y*,*z* stage (Owis GmbH, Staufen, Germany) with a resolution of 0.625 μm per half step and 48 nm per microstep. A PAR 273A potentiostat (Ametek, Oak Ridge, USA) with a bandwidth of 100 kHz was used. The voltage input of the potentiostat was connected to the oscillator output of a lock-in amplifier, while the current output went to the signal input of the latter. In contrast to the earlier work published in refs. [17,18,22,35], the read-out of phase-sensitive detection was achieved via the serial port using an EG&G 7280 digital lock-in amplifier (Ametek, Oak Ridge, USA) rather than through an analogue-to-digital converter. Hence, the applied frequency was not selected manually via the front panel menu, but digitally via the serial port of the lock-in amplifier. This enabled the frequency to be changed remotely by the computer during the course of an AC-SECM measurement. The in-house written control software in Visual Basic 3.0 (Microsoft, Unterschleißheim, Germany) was adapted accordingly.

Acknowledgement

This work was partially financially supported by the Deutsche Forschungsgemeinschaft in the framework of the Sonderforschungsbereich SFB 459 (project A5).

[1] A. J. Bard, F. R. F. Fan, J. Kwak, O. Lev, *Anal. Chem.* **1989**, *61*, 132–138.
[2] M. V. Mirkin, B. R. Horrocks, *Anal. Chim. Acta* **2000**, *406*, 119–146.
[3] G. Wittstock, M. Burchardt, S. E. Pust, Y. Shen, C. Zhao, *Angew. Chem.* **2007**, *119*, 1604–1640; *Angew. Chem. Int. Ed.* **2007**, *46*, 1584–1617.
[4] S. B. Basame, H. S. White, *Langmuir* **1999**, *15*, 819–825.
[5] T. E. Lister, P. J. Pinhero, *Electrochim. Acta* **2003**, *48–49*, 555–561.
[6] R. M. Souto, Y. Gonzalez-Garcia, S. Gonzalez, *Corros. Sci.* **2005**, *45*, 3312–3323.
[7] C. Gabrielli, S. Joiret, M. Keddam, H. Perrot, N. Portail, P. Rousseau, V. Vivier, *Electrochim. Acta* **2007**, *52*, 7706–7714.
[8] J. Kwak, A. J. Bard, *Anal. Chem.* **1989**, *61*, 1221–1227.
[9] R. D. Martin, P. R. Unwin, *J. Chem. Soc. Faraday Trans.* **1998**, *94*, 753–759.
[10] K. Eckhard, X. Chen, F. Turcu, W. Schuhmann, *Phys. Chem. Chem. Phys.* **2006**, *8*, 5359–5365.
[11] B. R. Horrocks, M. V. Mirkin, D. T. Pierce, A. J. Bard, G. Nagy, K. Toth, *Anal. Chem.* **1993**, *65*, 1213–1224.
[12] D. M. Osbourn, R. H. Sanger, P. J. S. Smith, *Anal. Chem.* **2005**, *77*, 6999–7004.
[13] B. R. Horrocks, D. Schmidtke, A. Heller, A. J. Bard, *Anal. Chem.* **1993**, *65*, 3605–3614.
[14] R. Kashyap, K. Gratzl, *Anal. Chem.* **1999**, *71*, 2814–2820.
[15] M. A. Alpuche-Aviles, D. O. Wipf, *Anal. Chem.* **2001**, *73*, 4873–4881.
[16] R. T. Kurulugama, D. O. Wipf, S. A. Takacs, S. Pongmayteegul, P. A. Garris, J. E. Baur, *Anal. Chem.* **2005**, *77*, 1111–1117.
[17] B. B. Katemann, A. Schulte, E. J. Calvo, M. Koudelka-Hep, W. Schuhmann, *Electrochem. Commun.* **2002**, *4*, 134–138.
[18] B. B. Katemann, C. G. Inchauspe, P. A. Castro, A. Schulte, E. J. Calvo, W. Schuhmann, *Electrochim. Acta* **2003**, *48*, 1115–1121.
[19] A. S. Baranski, P. M. Diakowski, *J. Solid State Electrochem.* **2004**, *8*, 683–692.
[20] C. Gabrielli, F. Huet, M. Keddam, P. Rousseau, V. Vivier, *J. Phys. Chem. B* **2004**, *108*, 11620–11626.
[21] G. Baril, G. Galicia, C. Deslouis, N. Pebere, B. Tribollet, V. Vivier, *J. Electrochem. Soc.* **2007**, *154*, c108–c113.
[22] M. Etienne, A. Schulte, W. Schuhmann, *Electrochem. Commun.* **2004**, *6*, 288–293.
[23] P. M. Diakowski, A. S. Baranski, *Electrochim. Acta* **2006**, *52*, 854–862.
[24] K. Eckhard, C. Kranz, H. Shin, B. Mizaikoff, W. Schuhmann, *Anal. Chem.* **2007**, *79*, 5435–5438.
[25] K. Eckhard, M. Etienne, A. Schulte, W. Schuhmann, *Electrochem. Commun.* **2007**, *9*, 1793–1797.
[26] K. Eckhard, W. Schuhmann, H. Shin, B. Mizaikoff, C. Kranz, *Electrochem. Commun.* **2007**, *9*, 1311–1315.

[27] E. N. Ervin, H. S. White, L. A. Baker, *Anal. Chem.* **2005**, *77*, 5564–5569.
[28] E. N. Ervin, H. S. White, L. A. Baker, C. R. Martin, *Anal. Chem.* **2006**, *78*, 6535–6541.
[29] A. M. Mierisch, S. R. Taylor, *J. Electrochem. Soc.* **2003**, *150*, b303–b308.
[30] A. M. Mierisch, S. R. Taylor, V. Celli, *J. Electrochem. Soc.* **2003**, *150*, b309–b315.
[31] K. Eckhard, W. Schuhmann, *Electrochim. Acta* **2007**, *52*, 1164–1169.
[32] C. Gabrielli, M. Keddam, N. Portail, P. Rousseau, H. Takenouti, V. Vivier, *J. Phys. Chem. B* **2006**, *110*, 20478–20485.
[33] C. Kranz, M. Ludwig, H. E. Gaub, W. Schuhmann, *Adv. Mater.* **1995**, *7*, 38–40.
[34] C. Kranz, M. Ludwig, H. E. Gaub, W. Schuhmann, *Adv. Mater.* **1995**, *7*, 568–571.
[35] A. Schulte, S. Belger, M. Etienne, W. Schuhmann, *Mater. Sci. Eng. A-Struct. Mater. Prop. Microstruct. Process.* **2004**, *378*, 523–526.

Received: November 26, 2007
Published online: March 20, 2008

